

## Hierarchical modelling of a polymer matrix composite

Joel P. Foreman · Shabnam Behzadi ·  
David Porter · Paul T. Curtis · Frank R. Jones

Received: 28 March 2008 / Accepted: 30 April 2008 / Published online: 31 July 2008  
© Springer Science+Business Media, LLC 2008

**Abstract** A hierarchical modelling scheme to predict the properties of a polymer matrix composite is introduced. The stress–strain curves of amine-cured tetraglycidyl 4,4'-diaminodiphenylmethane (TGDDM) cured have been predicted using group interaction modelling (GIM). The GIM method, originally applied primarily to linear polymers, has been significantly extended to give accurate, consistent results for TGDDM, a highly crosslinked two-component matrix. The model predicts a complete range of temperature-dependent properties, from fundamental energy contributions, through engineering moduli to full stress–strain curves through yield. The predicted properties compare very well with experiment. Using the GIM-predicted TGDDM stress–strain curve, a 3D finite element model is used to obtain strain concentration factors (SCF) of fibres adjacent to a fibre break in a unidirectional (UD) composite. The strain distribution among the intact neighbouring fibres is clearly affected by the yielding mechanism in the resin matrix. A Monte Carlo simulation is carried out to predict the tensile failure strain of a single composite layer with the thickness equal to the fibre ineffective length. The effect of matrix shear yielding is introduced to the model through the SCF of surviving

fibres adjacent to the fibre-break. The tensile failure strain of the composite is then predicted using a statistical model of a chain of composite layers.

### Introduction

Multi-functional epoxy resins are one of the most popular choices of matrix used in modern fibre-reinforced composite materials. When cured, an amorphous thermoset with superior strength and toughness, excellent corrosion and moisture resistance, good thermal and electrical properties and low shrinkage results [1]. Several commercial aerospace composites use matrices consisting of cured diglycidyl ethers or multi-functional glycidyl amines which exhibit excellent thermomechanical properties. One of the most commonly used epoxies is tetraglycidyl 4,4'-diaminodiphenylmethane (TGDDM, sold as Araldite MY721) which has four highly reactive epoxy sites. The tetrafunctional nature of both TGDDM and the curing agent diaminodiphenylsulphone (DDS) leads to the formation of a highly crosslinked 3D network. The curing mechanism is well-documented [2], but exact structural information about a TGDDM/DDS network is difficult to obtain.

The use of predictive modelling to estimate engineering properties of composites is becoming more popular [3]. This paper documents the design of a hierarchical approach to the modelling of composites. In the first stage, group interaction modelling (GIM) is used to predict a full set of thermomechanical and engineering properties of the matrix. This technique has previously been successfully applied to a wide variety of linear polymers [4] but its application to two-component branched polymers is limited [5]. The glass transition temperature of 924 epoxy

---

J. P. Foreman · S. Behzadi · F. R. Jones (✉)  
Ceramics and Composites Laboratory, Department  
of Engineering Materials, University of Sheffield,  
Mappin Street, Sheffield S1 3JD, UK  
e-mail: f.r.jones@sheffield.ac.uk

D. Porter  
Department of Zoology, University of Oxford,  
South Parks Road, Oxford OX1 3PS, UK

P. T. Curtis  
Physical Sciences Department, DSTL, 415 Building,  
Porton Down, Wilts SP4 0JQ, UK

resin was predicted using a similar GIM-based approach [6]. Other efforts to model highly crosslinking epoxies have used data from kinetic simulations and NIR spectra as input [7]. GIM has also been applied successfully to spider silk [8, 9] and concrete.

In a unidirectional (UD) fibre composite, the statistical strength distribution along the fibres results in a large discrepancy between the failure strength of a real composite and the one predicted from a simple rule of mixtures. Most of the leading predictive models of the composite failure are based on statistical methods which use the strength distribution along the fibres. However, overlooking the nonlinear behaviour of the matrix in the analytical models [10–12] has led to unreliable results and limited the capability of the models.

A fibre-break is a critical micro-event in a UD composite. The stress released by a fibre-break is re-distributed among the intact adjacent fibres to re-establish a local load equilibrium. The strain (or stress) concentration in adjacent fibres increases the probability of their fracture and hence controls the ultimate failure of the composite material. The strain (or stress) concentration factor (SCF) is a key parameter used in statistical models to predict the failure strength of a UD composite. It is believed that interfacial shear yielding of an elasto-plastic matrix governs the re-distribution of the overload among the intact fibres. This leads to a decrease in the probability that a crack will propagate through the matrix as well as reducing the SCF in the adjacent fibres [13, 14]. Therefore, the behaviour of an elasto-plastic matrix under load can alter the micromechanics of the fracture in a fibre composite.

Several models have been proposed for the prediction of the strength of UD composites, two of which are key. Firstly, Rosen's model [10] which considers the equal load sharing rule between fibres and a matrix which only carries a shear load. This model predicted significantly higher failure strength than that of real composites. Secondly, Zweben's model [11] which used the SCF values suggested by Hedgepeth and Van Dyke [15] and reported a lower strength than that of a real composite. This could be attributed to the high SCF values obtained by the analytical methods. Wada and Fukuda [16] suggested that Rosen and Zweben's models are able to predict the upper and the lower bounds of the composite failure strength. Most of the statistical models [16–22] for composite failure strength are based on the linkage of several single fibre elements of a given ineffective length and incorporated into a Monte Carlo simulation.

Curtis [22] established an uncomplicated model which predicts the progressive growth of fibre breaks and the failure strain of UD composites under tension. This study did not take into account the effect of a yielding matrix in the model. Thus it is essential to establish a link between

the matrix yield properties and the ultimate failure strength of UD composites by determining the strain concentration factors in neighbouring fibres at the vicinity of a fibre-break. This paper details attempts to predict the failure strain of a UD composite including the GIM-predicted matrix yield properties using the Curtis model.

## Methods

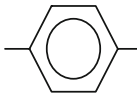

### Group interaction modelling

In group interaction modelling interactions between neighbouring polymer chains are defined using a potential function that consists of several thermodynamic energy terms. The energy balance between attractive, cohesive energy,  $E_{\text{coh}}$ , and repulsive, thermal energy,  $H_T$ , represents the equation of state for the system under investigation. This is shown in Eq. 1 where the total GIM energy,  $E_{\text{total}}$ , is defined.

$$E_{\text{total}} = 0.89 E_{\text{coh}} - H_T \quad (1)$$

The set of fundamental parameters required for input into GIM is based around the representative mer unit. These are the degrees of freedom,  $N$ , the cohesive energy at absolute zero,  $E_{\text{coh}}(0 \text{ K})$ , the van der Waal's volume,  $V_w$ , the length,  $L$ , the molecular weight,  $M$ , and the Debye temperature,  $\theta_1$ . The degrees of freedom,  $N$ , is the most important of the parameters in GIM and care must be taken in its evaluation. Initial values are taken from group contributions such as shown in Table 1. The incorporation of crosslinking into the model is achieved by reducing the value of  $N$  by 3 for each crosslinking site on the mer unit.

**Table 1** GIM input parameters including functional group and uncured mer unit contributions

	$N$	$E_{\text{coh}}(0 \text{ K})$ (J/mol)	$V_w$ (cm <sup>3</sup> /mol)
CH <sub>2</sub>	2	4,500	10.25
	3	25,000	43.3
N	2	9,000	4
	4	15,300	22
CH(OH)	2	20,800	11.5
SO <sub>2</sub>	2	45,000	20.3
TGDDM mer unit	36	191,700	232.9
DDS mer unit	12	113,000	114.9

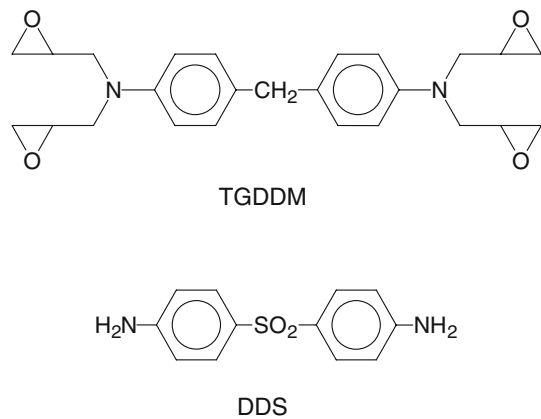


**Fig. 1** Chemical structures of TGDDM and DDS

The other five input parameters are taken from the functional group contributions in Table 1 and summed to give mer unit values. All the input parameters are evaluated for the epoxy and amine mer units based on their molecular structures as shown in Fig. 1. The parameters for the two components are then combined to give parameters for the cured resin mer unit. For TGDDM cured with DDS, the epoxy and amine are combined in a stoichiometric ratio of 1:1 as both components have four reactive sites. The GIM parameters for the cured TGDDM/DDS mer unit are given in Table 2.

In TGDDM/DDS two distinct transition temperatures occur in the dynamic mechanical response. The well-known glass transition at  $\sim 275$  °C is due to a sharp increase in intermolecular motion as the polymer chains become capable of independent movement. The low temperature beta transition at  $\sim -100$  °C is less well defined and is believed to be associated with an intramolecular crankshaft style motion of the phenyl–phenyl segments [23]. The transitions are modelled using normal distribution functions which require a characteristic temperature and the cumulative loss through the transition. The glass transition temperature is predicted using Eq. 2 where  $r$  is the strain rate and  $f$  is the characteristic vibrational frequency of the polymer chain. The characteristic frequency of the chain is obtained from  $k\theta_1 = hf$  where  $k$  and  $h$  are the Boltzmann and Planck constants, respectively. The

**Table 2** GIM input parameters for the cured TGDDM/DDS mer unit

Input parameter	
$N$	18
$E_{\text{coh}}$ (0 K) (J/mol)	152,350
$V_w$ (cm <sup>3</sup> /mol)	173.9
$L$ (Å)	14
$M$	333
$\theta_1$ (K)	550

**Table 3** Comparison between predicted and experimental properties for TGDDM/DDS. All properties are measured at room temperature at a strain rate of 1 Hz with the exception of  $E$  and  $\sigma_y$  which are at 0.00167 Hz. Experimental values of  $T_g$ ,  $T_\beta$  and  $\rho$  are taken from reference [5],  $\alpha_1$  is taken from reference [33],  $E$  and  $\sigma_y$  are taken from reference [34]

Property	GIM predicted	Experimental
$T_g$ (°C)	281	270
$T_\beta$ (°C)	−38	−45
$\rho$ (g/cm <sup>3</sup> )	1.30	1.29
$\alpha_1$ ( $\times 10^{-6}$ /K)	50	$\sim 50$
$E$ (GPa)	5.17	5.04
$\sigma_y$ (MPa)	201	200

GIM-predicted  $T_g$  compares well with the experimental values as shown in Table 3.

$$T_g = 0.224 \theta_1 + \frac{0.0513 E_{\text{coh}} (0\text{K})}{N} - 50 + \frac{1280 + 50 \ln \theta_1}{\ln \left( \frac{2\pi f}{r} \right)} \quad (2)$$

The beta temperature can be predicted using an Arrhenius equation as shown in Eq. 3. The activation energy for the beta transition,  $-\Delta H_\beta$ , is obtained using a simple quantum mechanics routine that estimates the phenyl ring rotation energy in epoxy systems and  $R$  is the gas constant. The GIM-predicted beta transition temperature value is given in Table 3 and compares very well with experiment.

$$T_\beta = \frac{-\Delta H_\beta}{R \ln \left( \frac{r}{2\pi f} \right)} \quad (3)$$

The cumulative loss tangent through the beta transition can be estimated using the ratio of the energy lost to the energy stored through an individual beta event. Equation 4 represents the ratio of energy required to perform the beta transition to the energy evolved as heat during the process.  $\Delta N$  and  $\Delta T$  represent the change in degrees of freedom and temperature through the transition, respectively.

$$\tan \Delta_\beta = \frac{R \Delta N T_\beta}{R N \Delta T} \quad (4)$$

Both transitions are modelled using their characteristic temperature, their cumulative loss tangent and an appropriate distribution term to give the correct peak shape.

#### Finite element model

A 3D fibre composite was modelled by Ansys 10.1 [24] containing six hexagonally packed carbon fibres enclosed by the TGDDM/DDS resin matrix. The fibre volume fraction of 50% was fixed by adjusting the distance between the fibres. Perfect interfacial bonding was achieved between the fibres and the matrix by ensuring coincidence of nodes along the

fibre/matrix interfaces in the model. GIM-predicted matrix properties were introduced into the model using the compressive stress–strain curve of the resin. The multi-linear elasticity option was chosen to represent the elasto-plastic behaviour of the resin. The properties of the transversely orthotropic HTA5131 carbon fibres (Diameter = 7 μm,  $E_z = 235$  GPa,  $E_x = E_y = 13.8$  GPa,  $\nu_{yx} = 0.35$ ,  $\nu_{zy} = \nu_{zx} = 0.2$ ,  $G_{xy} = 5.11$  GPa,  $G_{yz} = G_{xz} = 18$  GPa) used in this model were taken from reference [25]. The eight-noded solid brick structural element, SOLID45, was employed to mesh both the fibres and the matrix in the model. In a static FE model, a fibre-break can be introduced into the model prior to the loading, as it is equivalent to the fracture of the fibre during loading. The top layer of the elements can be removed from the fibre-end as shown in Fig. 2. The meshing in the region adjacent to the induced fibre-break was refined for both fibres and matrix. An axial displacement of 1% was applied on the front face of the model in z-direction while the back face was constrained with  $z = 0$ . The model was constrained on its other faces to ensure stability. Moreover, the nodes at the rim of the fibre-break in the matrix were constrained at UX and UY to prevent rotation during deformation. A strain analysis was carried out because of the known failure response of these composites.

Statistical model

The model consisted of 20 fibres in a layer of UD composite of thickness equal to the ineffective length of the fibre. Each fibre adopted a failure strain randomly from a normal distribution generated by the Box–Muller method [26]. The normal random fibre failure strains,  $\epsilon_i$ , are obtained by the following equation:

$$\epsilon_i = \mu + z_i\sigma \tag{5}$$

where  $\mu$  and  $\sigma$  are the mean and standard variation of fibre failure strains at an ineffective length and  $z_i$  are the normal

random numbers with a mean value of 0 and a standard deviation of 1. The mean strain of a fibre of an ineffective length was obtained by extrapolating the data for longer lengths [27]. A coefficient of variation of 20% was used in the analysis.

In the model procedure, the weakest fibre in the layer is found and the applied strain is increased to match the failure strain of the fibre. As a result of the fibre fracture, an overload is shed equally among its six intact nearest neighbouring fibres according to the strain concentration factor. With two adjacent fibres broken, the overload shed by these fibres is transferred onto the eight adjacent fibres and so on. The local strain concentration is updated after each fibre-break for all surrounding fibres. Therefore, the number of fibres affected by the failures continuously changes with the occurrence of new fibre-breaks. The procedure is repeated until an unstable crack occurs and the fibres start to fail successively without an increase in the applied strain, and thus the layer fails. The applied strain at this stage is taken as the failure strain of the composite layer. The programme can be ended when 2–3% of the fibres in a layer have failed [22].

In the next stage, a fixed number of the single layers are stacked together to form a piece of UD composite of a known length. However, in this preliminary study, the interaction between the single layers is not considered. The failure is assumed to occur when random fibre breaks have weakened one layer so that it can no longer withstand the applied load. The average failure strain of a known size of composite,  $\bar{\epsilon}_{\text{composite}}$ , can be found from the re-arranged form of Eq. 5 below

$$\bar{\epsilon}_{\text{composite}} = \bar{\epsilon}_{\text{lf}} - z_1\sigma_1 \tag{6}$$

where  $\bar{\epsilon}_{\text{lf}}$  is the average failure strain of the layers,  $z_1$  is the probability of layer failure and  $\sigma_1$  is the standard deviation of failure strain in the layers.

Results and discussions

Thermomechanical properties of TGDDM/DDS

The total GIM energy is predicted by estimating the energy terms in Eq. 1. The heat capacity of the cured mer unit,  $C_p$ , is determined using the Tarasov extension to the Debye model [28, 29] in Eq. 7. The heat capacity is then integrated to give the thermal energy,  $H_T$ , which is plotted against temperature for TGDDM/DDS in Fig. 3.

$$C_p = NR \frac{\left(\frac{6.7T}{\theta_1}\right)^2}{1 + \left(\frac{6.7T}{\theta_1}\right)^2} \tag{7}$$

The temperature-dependent cohesive energy,  $E_{\text{coh}}$ , is estimated by modifying the mer unit value at absolute zero,

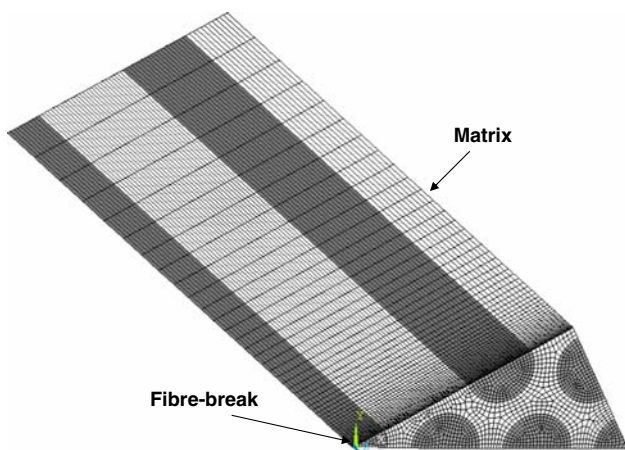
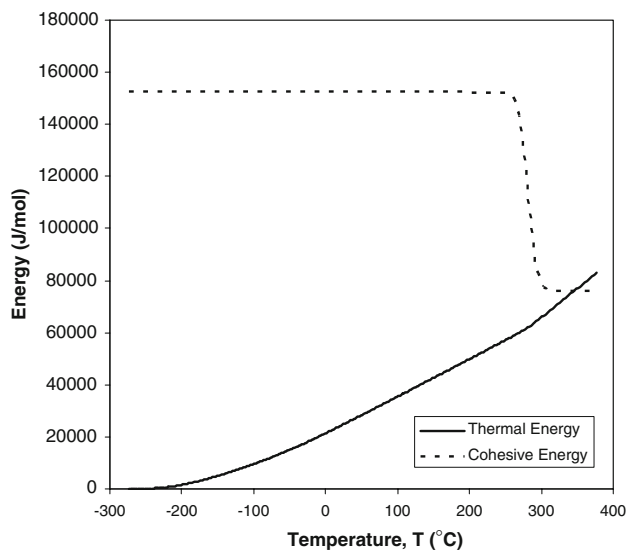


Fig. 2 The meshed FE model



**Fig. 3** GIM-predicted thermal energy ( $H_T$  in J/mol, solid) and cohesive energy ( $E_{coh}$  in J/mol, dotted) for TGDDM/DDS. A strain rate of 0.00167 Hz was used at room temperature

$E_{coh}$  (0 K), which was given in Table 2. This is done using a normal distribution function and assuming a 50% energy loss over the glass transition. Figure 3 also shows  $E_{coh}$  against  $T$  for TGDDM/DDS and the two plots together give an indication of the change in total energy in the polymer with rising temperature. The beta transition is practically invisible in the thermal energy line because it is a relatively low-energy phenomenon spread over a large temperature range. In contrast, the glass transition is seen as a change in gradient in the thermal energy function and a significant drop in the cohesive energy.

The volumetric thermal expansion coefficient,  $\alpha_v$ , is predicted using Eq. 8 which is then integrated over temperature to give the volume of the mer unit,  $V$ . This is plotted against temperature for TGDDM/DDS in Fig. 3 and again, only the glass transition is evident as a change in gradient in the volume line. The volume of the mer unit can be checked experimentally by comparing the predicted and measured density [5]. Table 3 shows the GIM-predicted density and linear thermal expansion coefficient,  $\alpha_l$ , compares very well with experiment.

$$\alpha_v = \frac{1.38 C_p}{R E_{coh}} \quad (8)$$

The bulk modulus,  $B$ , is given using Eq. 9 where  $E_{total}$  is the total GIM energy from Eq. 1. The predicted bulk modulus is shown against temperature for TGDDM/DDS in Fig. 4 where the two drops in the bulk modulus centred on  $T_\beta$  and  $T_g$  correspond to the two transitions. The beta transition shows a characteristically large temperature range ( $\sim 200$  °C), while the glass transition occurs over a smaller temperature range ( $\sim 10$  °C).

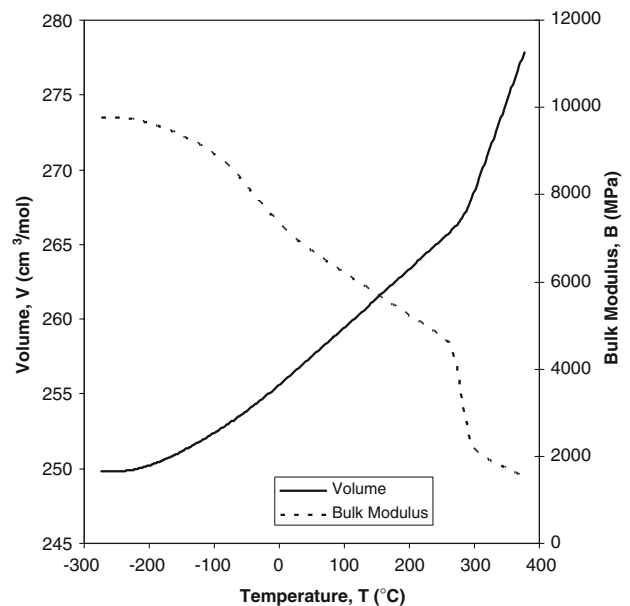


**Fig. 4** GIM-predicted volume ( $V$  in  $\text{cm}^3/\text{mol}$ , solid) and bulk modulus ( $B$  in MPa, dotted) for TGDDM/DDS. A strain rate of 0.00167 Hz was used at room temperature

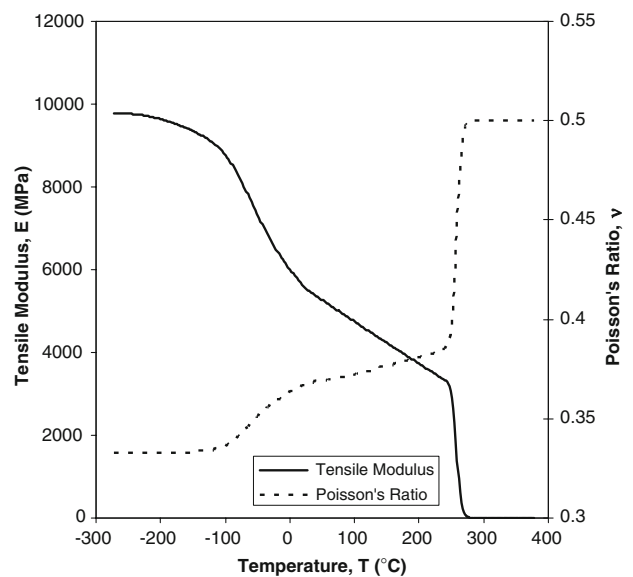


**Fig. 5** GIM-predicted tensile modulus ( $E$  in MPa, solid) and Poisson's ratio ( $\nu$ , dotted) for TGDDM/DDS. A strain rate of 0.00167 Hz was used at room temperature

$$B = 18 \frac{E_{total}}{V} \quad (9)$$

The Young's modulus in tension,  $E$ , is given by Eq. 10 where  $\tan\Delta_\beta$  is the cumulative loss tangent through the beta transition and  $A$  is a loss factor constant. The predicted modulus is plotted against temperature for TGDDM/DDS in Fig. 5 where it varies with temperature in a similar fashion to the bulk modulus, showing the two clear losses

at the beta and glass transitions. The predicted modulus at room temperature compares very well to the experimental value given in Table 3. It is worth noting that the predicted modulus is in tension while the experimental data used for comparison is in compression. The two values are practically identical at the relatively low strain values used in this work [30].

$$E = B \exp\left(\frac{-\tan \Delta\beta}{AB}\right) \quad \text{where} \quad A = \frac{15L}{\theta_1 M} \quad (10)$$

The bulk and tensile moduli are combined to give a predicted value of Poisson’s ratio,  $\nu$ , which is also plotted against temperature in Fig. 5. At low temperatures the polymer is brittle ( $\nu < 0.37$ ), at high temperatures it is ductile ( $\nu > 0.38$ ) and between room temperature and 180 °C,  $\nu$  varies by as little as  $\sim 0.01$ . Commercial epoxy resins such as MY721 are designed to have a Poisson’s ratio around 0.37–0.38 on the brittle/ductile threshold and this is well predicted by the model.

### Stress–strain curves for TGDDM/DDS

The elastic strain,  $\varepsilon_e$ , is predicted using Eq. 11 where the predicted thermal expansion coefficient is converted into strain. Energy dissipation is taken into account by including plastic flow effects by means of the loss tangent,  $\tan \delta$  to give the full strain,  $\varepsilon$ , in Eq. 11.

$$\varepsilon_e = \int_{T_0}^T \alpha_1 dT \quad (11)$$

$$\varepsilon = \varepsilon_e \left( 1 + \int_0^T \tan \delta dT \right) \quad (12)$$

The Young’s modulus over the full strain gives a prediction of the stress in tension. Finally, the compressive stress,  $\sigma_c$ , is predicted using Eq. 13 where twice the Poisson’s ratio has been used to correct for expansion in the two axes normal to the compression. Compressive stress is plotted against strain in Fig. 6 for TGDDM/DDS along with an experimental comparison.

$$\sigma_c = \frac{\int_{T_0}^T E \alpha_1 \left( 1 + \int_0^T \tan \delta dT \right) dT}{2\nu} \quad (13)$$

Overall, the GIM-predicted stress–strain curve compares very well to the experimental plot. The predicted pre-yield section is very close to experiment including subtle changes in gradient as the yield condition commences. The yield point is then reached at similar values of stress and strain in both the model and experiment. For the purposes of this work, the yield point is defined as the point on the stress–strain curve where the gradient first equals zero. The

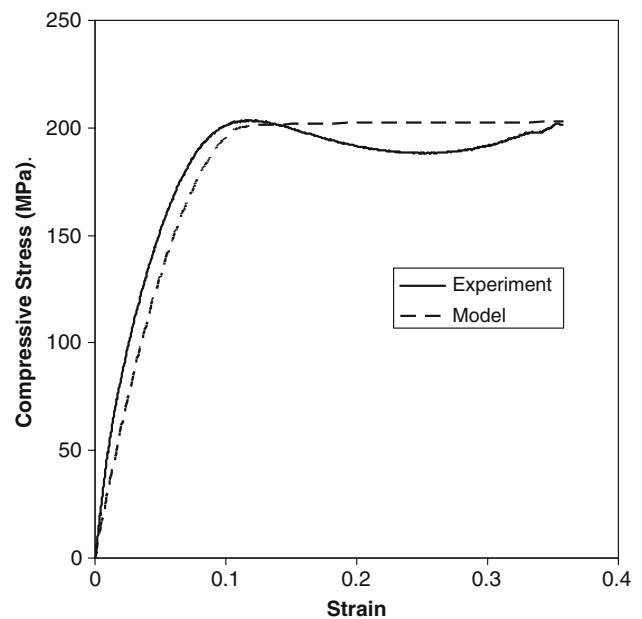


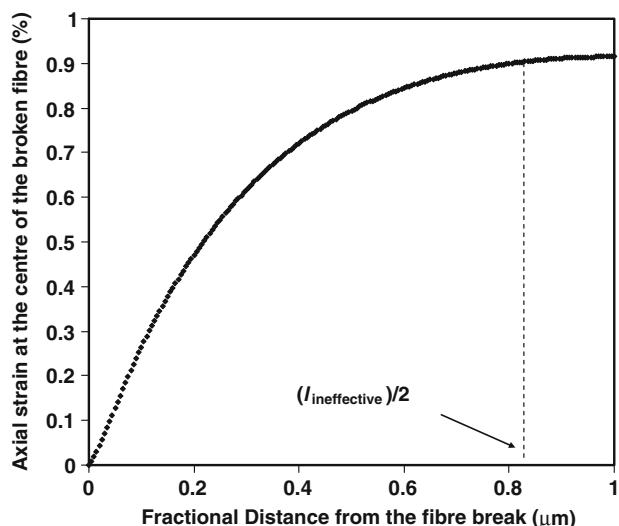
**Fig. 6** Comparison between the experimental (solid) and GIM-predicted (points) compressive stress–strain curve for TGDDM/DDS. A strain rate of 0.00167 Hz was used at room temperature. Experimental data were taken from Reference [34]

predicted and experimental yield stress compare very well, as shown in Table 3. In the experimental curve, the post-yield section includes a period of strain-softening and strain-hardening which is not currently included in the model.

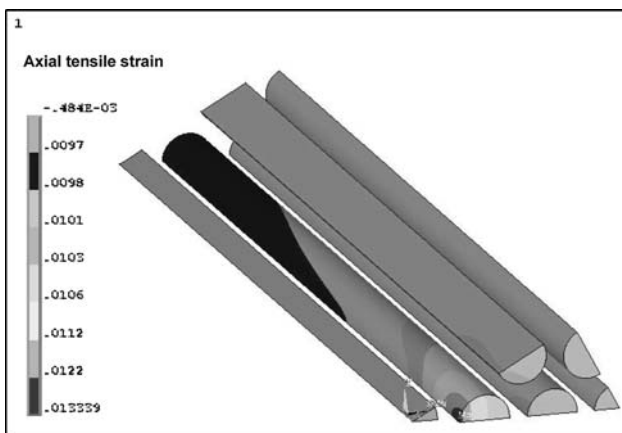
### Finite element analysis of fibre breakage

Figure 7 shows the development of the axial tensile strain along the centre of the broken fibre. It can be seen that the yielding of the matrix has resulted in an exponential increase in the broken fibre axial tensile strain following fibre fracture. Because of the elasto-plastic behaviour of the matrix, the applied strain cannot be fully recovered even at the far-field level from the broken fibre, so it falls below the applied strain of 1%. The ineffective length of the fibre can be considered as twice the length of the fibre fragment over which 90% of strain recovery occurred. The ineffective length of 0.161 mm (corresponds to 0.0805 mm  $\times$  2, obtained from Fig. 7) is within the range of values reported in the literature [31].

The introduction of a break leads to a considerable increase in axial strain around the break. Figure 8 shows the regions of intensified strain in the surrounding fibres in the plane of fracture. However, the SCF of the adjacent fibre is considered as the ratio of the averaged axial strain at its cross section to the applied strain. Table 4 shows the strain concentrations obtained for the surrounding fibres of a fibre-break. This shows that the SCF on the next-nearest



**Fig. 7** The axial tensile strain profile away from a fibre-break at the centre of the broken fibre within a hexagonal array at an applied strain of 1%



**Fig. 8** Contour map of the axial tensile strain in hexagonally packed fibres with a fibre-break showing strain concentrations in the nearest and next nearest neighbouring fibres. The resin matrix is not shown

**Table 4** The strain concentration factor in the neighbouring fibres of a broken fibre in the FE model of an UD composite containing the TGDDM/DDS resin matrix

Fibre geometry	Nearest neighbour	Next-Nearest neighbour
Hexagonal	1.11	1.009

neighbouring fibres (at 1.009) is almost one and can therefore be disregarded.

The elasto-plasticity of the matrix has been incorporated into a FE model and led to a significant decrease in strain concentration factor in the fibres in comparison with the non-yield (elastic) matrix case which is considered to be 1.17 [14]. As the elasto-plastic matrix at the vicinity of a broken fibre absorbs energy to deform plastically, it

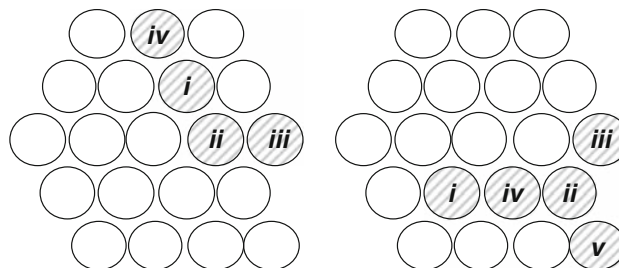


**Fig. 9** The sequence of fibre failure (numbered) in two examples of a fibre composite layer with different random fibre failure distributions. White and shaded fibres represent intact and broken fibres, respectively

**Table 5** The effect of SCF in the fibres on the layer failure strain and the size of stable group of broken fibres (the layer thickness is 0.161 mm)

SCF	1.11
Fibre failure strain (%) [27]	2.47 ± 0.49
Layer strain at the first fibre failure (%)	1.42 ± 0.25
Layer failure strain (%)	1.83 ± 0.16
Mean size of stable group of broken fibres	1.5 ± 0.9

reduces the stress concentration on the intact adjacent fibres of a broken fibre [32]. This reduces the probability of failure of the adjacent fibres and eventually of the UD composite material.

Statistical model of a UD composite

The statistical program is applied to a layer of fibre composite with ineffective length, 0.161 mm, incorporating the effect of yielding TGDDM/DDS resin matrix. Figure 9 shows two examples of fibre failure sequence in typical composite layers. Initially, stable groups of broken fibres form in the layer that withstand the overload imposed by the broken fibres, which then become unstable at higher applied strains. Therefore, the failure strain of the layer is determined by the weakest fibre when failure begins. Table 5 shows the mean failure strain of the composite layer and the average size of the largest stable group of broken fibres. It was assumed that a specific number of single layers with a random distribution of failure strains are stacked to make a fibre composite. Figure 10 shows the change in failure strain of the 3D composite with logarithmic length. The failure strain becomes independent of length above a few centimetres.

In this preliminary study, it is assumed that all neighbouring fibres around fractured fibres share an equal overload regardless of their absolute distances from the crack. The composite failure strain predicted in this preliminary study is greater than typical experimental values

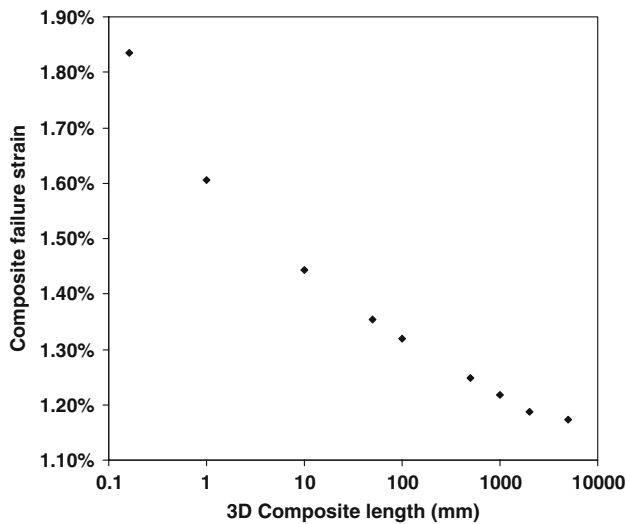


**Fig. 10** The complete multiscale prediction of the failure strain of a unidirectional carbon fibre composite as a function of length

(nearly 1.12%) for a given length of composite [22]. This may be associated with the choice of ineffective length. It has been demonstrated that a slight increase in the layer thickness decreases the composite failure strain and results in a better agreement with experiment. Interaction between layers may also be significant and has not been taken into account in this analysis.

**Conclusions**

A hierarchical approach to the modelling of a complete composite system has been described. The thermomechanical and engineering properties of a popular epoxy matrix have been predicted and used as input into finite element analysis. The re-distribution of strain concentration upon fibre breakage has been assessed using a statistical model.

Group interaction modelling of polymers which has previously concentrated on linear systems has been revised and extended. It is now capable of predicting the thermomechanical and engineering properties of a highly crosslinking, two-component amine-cured epoxy resin system. Moreover, the single property-targeted approach of previous works has been extended so that the model now predicts properties over a full temperature range from fundamental energy contributions right up to moduli and stress–strain curves. Predicted properties for amine-cured TGDDM compare very well with experiment.

The yield behaviour of the resin matrix was linked to the probability of failure of a UD fibre composite. The shear yielding of the matrix reduced the strain concentration factor in the fibres at the vicinity of a fibre fracture

compared to a non-yield matrix. The failure strain of a 3D fibre composite has been predicted based on the weakest link theory using the failure strain of the composite layers. A better agreement between the predicted failure strain and experiment requires a detailed study of the influence of the ineffective length of the fibres.

**Acknowledgements** This work was carried out as part of Weapons and Platform Effectors Domain of the MoD Research Program. The authors would like to thank the UK EPSRC for part funding of this project.

**Glossary**

<i>A</i>	Loss factor
<i>B</i>	Bulk modulus
<i>C<sub>p</sub></i>	Heat capacity
<i>E</i>	Young’s modulus in tension
<i>E<sub>total</sub></i>	Total GIM energy
<i>E<sub>coh</sub></i>	Cohesive energy
<i>E<sub>coh</sub> (0 K)</i>	Cohesive energy at 0 K
<i>f</i>	Characteristic vibrational frequency of the polymer chain
<i>H<sub>T</sub></i>	Thermal energy
$\Delta H_\beta$	Activation energy of the beta transition
<i>h</i>	Planck’s constant
<i>k</i>	Boltzmann’s constant
<i>L</i>	Length of the mer unit
<i>M</i>	Molecular weight of the mer unit
<i>N</i>	Degrees of freedom
$\Delta N$	Degrees of freedom change for a single beta event
<i>R</i>	Gas constant
<i>r</i>	Strain rate
<i>T</i>	Temperature
<i>T<sub>g</sub></i>	Glass transition temperature
<i>T<sub>β</sub></i>	Beta transition temperature
$\Delta T$	Temperature change for a single beta event
$\tan\Delta_\beta$	Cumulative loss tangent through the beta transition
$\tan\delta$	Local total loss tangent
<i>V</i>	Volume of the mer unit
<i>V<sub>w</sub></i>	van der Waal’s volume of the mer unit
<i>z<sub>i</sub></i>	Normal random numbers
<i>z<sub>l</sub></i>	Probability of layer failure
$\alpha_l$	Linear thermal expansion coefficient
$\alpha_v$	Volumetric thermal expansion coefficient
$\epsilon$	Full strain
$\epsilon_e$	Elastic strain contribution
$\bar{\epsilon}_{composite}$	Average failure strain of a size of composite
$\bar{\epsilon}_{if}$	Average failure strain of composite layer
$\mu$	Mean fibre failure strain



$\nu$	Poisson's ratio
$\theta_1$	Debye temperature normal to polymer chain axis
$\rho$	Density
$\sigma$	Standard fibre failure strain
$\sigma_c$	Compressive stress
$\sigma_1$	Standard deviation of layer failure strain
$\sigma_y$	Compressive yield stress

## References

- Pham HQ, Marks MJ (2002) Epoxy resins. In: Encyclopedia of polymer science and technology. Wiley
- Gupta A, Cizmecioglu M, Coulter D, Liang RH, Yavrouian A, Tsay FD, Moacanin J (1983) *J Appl Polym Sci* 28:1011. doi: [10.1002/app.1983.070280309](https://doi.org/10.1002/app.1983.070280309)
- Jones FR (2005) In: Soutis C, Beaumont PWR (eds) Multi-scale modelling of composite material systems: the art of predictive damage modelling. Woodhead publishing limited, Cambridge, p 528
- Porter D (1995) Group interaction modelling of polymer properties. Marcel Dekker, New York
- Foreman JP, Porter D, Behzadi S, Travis KP, Jones FR (2006) *J Mater Sci* 41:6631. doi: [10.1007/s10853-006-0202-9](https://doi.org/10.1007/s10853-006-0202-9)
- Gumen VR, Jones FR, Attwood D (2001) *Polymer* 42:5717. doi: [10.1016/S0032-3861\(00\)00930-7](https://doi.org/10.1016/S0032-3861(00)00930-7)
- Liu HP, Uhlherr A, Bannister MK (2004) *Polymer* 45:2051. doi: [10.1016/j.polymer.2004.01.008](https://doi.org/10.1016/j.polymer.2004.01.008)
- Porter D, Vollrath F, Shao Z (2005) *Eur Phys J E* 16:199. doi: [10.1140/epje/e2005-00021-2](https://doi.org/10.1140/epje/e2005-00021-2)
- Vollrath F, Porter D (2006) *Appl Phys A-Mater Sci Process* 82:205. doi: [10.1007/s00339-005-3437-4](https://doi.org/10.1007/s00339-005-3437-4)
- Rosen BW (1964) *AIAA J* 2:1985
- Zweben C (1968) *AIAA J* 6:2325
- Zweben C, Rosen W (1970) *J Mech Phys Solids* 18:189. doi: [10.1016/0022-5096\(70\)90023-2](https://doi.org/10.1016/0022-5096(70)90023-2)
- Lane R, Hayes SA, Jones FR (2001) *Compos Sci Technol* 61:565. doi: [10.1016/S0266-3538\(00\)00229-3](https://doi.org/10.1016/S0266-3538(00)00229-3)
- Behzadi S, Curtis PT, Jones FR (2007) Proceedings of ICCM-16, Kyoto
- Hedgepeth JM, van Dyke P (1967) *J Compos Mater* 1:294
- Wada A, Fukuda H (1999) *Compos Sci Technol* 59:89. doi: [10.1016/S0266-3538\(98\)00052-9](https://doi.org/10.1016/S0266-3538(98)00052-9)
- LienKamp M, Schwartz P (1993) *Compos Sci Technol* 46:139. doi: [10.1016/0266-3538\(93\)90169-H](https://doi.org/10.1016/0266-3538(93)90169-H)
- Fukuda H, Kawata K (1977) *Fibre Sci Technol* 10:53. doi: [10.1016/0015-0568\(77\)90028-8](https://doi.org/10.1016/0015-0568(77)90028-8)
- Manders PW, Bader MG, Chou TW (1982) *Fibre Sci Technol* 17:183. doi: [10.1016/0015-0568\(82\)90003-3](https://doi.org/10.1016/0015-0568(82)90003-3)
- Ochiai S, Osamura K (1988) *J of Mater Sci* 23:886. doi: [10.1007/BF01153984](https://doi.org/10.1007/BF01153984)
- Curtin WA, Takeda N (1998) *J Compos Mater* 32:2060
- Curtis PT (1986) *Compos Sci Technol* 27:63. doi: [10.1016/0266-3538\(86\)90063-1](https://doi.org/10.1016/0266-3538(86)90063-1)
- Williams JG (1979) *J Appl Polym Sci* 23:3433. doi: [10.1002/app.1979.070231201](https://doi.org/10.1002/app.1979.070231201)
- ANSYS Inc.: reference manual, 2006
- Nedele MR (1996) In: Department of Aerospace Engineering, University of Bristol, Bristol
- Box GEP, Muller ME (1958) *Ann Math Stat* 29:610. doi: [10.1214/aoms/1177706645](https://doi.org/10.1214/aoms/1177706645)
- Bader MG, Priest AM (1982) ICCM-IV, Tokyo, pp 1159–1136
- Tarasov VV (1965) *Russ J Phys Chem* 39:1109
- Tarasov VV (1953) *Zh Fiz Khim* 27:1430
- Kozey VV, Kumar S (1994) *J Mater Res* 9:2717. doi: [10.1557/JMR.1994.2717](https://doi.org/10.1557/JMR.1994.2717)
- Phoenix SL, Schwartz P, Robinson HH (1988) *Compos Sci Technol* 32:81. doi: [10.1016/0266-3538\(88\)90001-2](https://doi.org/10.1016/0266-3538(88)90001-2)
- Behzadi S (2006) PhD thesis, Department of Engineering Materials, University of Sheffield, Sheffield
- Caballero-Martinez MI (2004) PhD thesis, Department of Engineering Materials, University of Sheffield, Sheffield, p 217
- Behzadi S, Jones FR (2005) *J Macromol Sci-Part B: Phys* 44:993